

Analyst

Accepted Manuscript



This is an *Accepted Manuscript*, which has been through the Royal Society of Chemistry peer review process and has been accepted for publication.

Accepted Manuscripts are published online shortly after acceptance, before technical editing, formatting and proof reading. Using this free service, authors can make their results available to the community, in citable form, before we publish the edited article. We will replace this *Accepted Manuscript* with the edited and formatted *Advance Article* as soon as it is available.

You can find more information about *Accepted Manuscripts* in the [Information for Authors](#).

Please note that technical editing may introduce minor changes to the text and/or graphics, which may alter content. The journal's standard [Terms & Conditions](#) and the [Ethical guidelines](#) still apply. In no event shall the Royal Society of Chemistry be held responsible for any errors or omissions in this *Accepted Manuscript* or any consequences arising from the use of any information it contains.

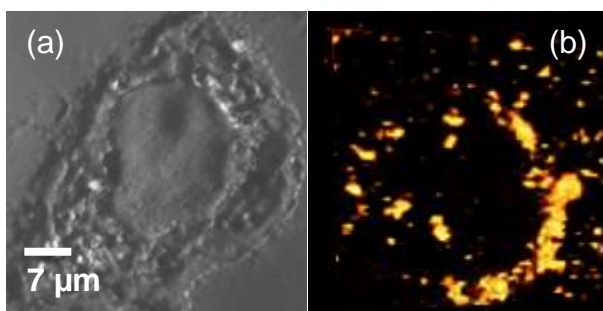
1
2
3
4
5
6
7
8
9
10
11
12
13
14
15
16
17
18
19
20
21
22
23
24
25
26
27
28
29
30
31
32
33
34
35
36
37
38
39
40
41
42
43
44
45
46
47
48
49
50
51
52
53
54
55
56
57
58
59
60

Table of contents entry for:

A carbon nanotube-based Raman-imaging immunoassay for evaluating tumor targeting ligands

Pooja Bajaj, Carole Mikoryak, Ruhung Wang, David K. Bushdiecker II, Pauras Memon, Rockford K. Draper, Gregg R. Dieckmann, Paul Pantano, and Inga H. Musselman*

Distribution of membrane receptors using targeting antibody immunoassay: (a) optical image; (b) G-band signal of carbon nanotubes as Raman label.



1
2
3 **A carbon nanotube-based Raman-imaging immunoassay for evaluating**
4 **tumor targeting ligands** †
5
6
7

8
9 **Pooja Bajaj,^a Carole Mikoryak,^b Ruhung Wang,^{ab} David K. Bushdiecker II,^a Pauras**
10 **Memon,^a Rockford K. Draper,^{abc} Gregg R. Dieckmann,^{ac} Paul Pantano,^{ac} and Inga H.**
11 **Musselman^{*ac}**
12
13
14

15
16
17
18 *^aDepartment of Chemistry, The University of Texas at Dallas, Richardson, TX 75080-3021,*
19 *USA. E-mail: imusselm@utdallas.edu*
20

21
22 *^bDepartment of Molecular and Cell Biology, The University of Texas at Dallas, Richardson,*
23 *TX 75080-3021, USA*
24

25
26
27 *^cThe Alan G. MacDiarmid NanoTech Institute, The University of Texas at Dallas, Richardson,*
28 *TX 75080-3021, USA*
29

30
31 † *Electronic supplementary information (ESI) available. See DOI: _____*
32
33
34

35
36 Herein, we describe a versatile immunoassay that uses biotinylated single-walled carbon
37 nanotubes (SWNTs) as a Raman label, avidin-biotin chemistry to link targeting ligands to the
38 label, and confocal Raman microscopy to image whole cells. Using a breast tumor cell
39 model, we demonstrate the usefulness of the method to assess membrane receptor/ligand
40 systems by evaluating a monoclonal antibody, Her-66, known to target the Her2 receptors
41 that are overexpressed on these cells. We present two-dimensional Raman images of the
42 cellular distribution of the SWNT labels corresponding to the distribution of the Her2
43 receptors in different focal planes through the cell with validation of the method using
44 immunofluorescence microscopy, demonstrating that the Her-66-SWNT complexes were
45 targeted to Her2 cell receptors.
46
47
48
49
50
51
52
53
54
55
56
57
58
59
60

Introduction

Targeted therapies are designed to selectively deliver a therapeutic agent to a specific molecular target, thereby providing a more effective treatment with fewer side effects. They are now incorporated in the treatment strategy of many common malignancies including breast, colorectal, lung, and pancreatic cancers, as well as lymphoma, leukemia, and myeloma.¹ Recently, the efficacy of targeted therapies has improved through the use of nanoparticles that can package drugs with a controlled size, shape, and surface chemistry to enhance their solubility, bioavailability, and residence times.² An ancillary benefit of using nanoparticles is that many can additionally serve as an imaging label (e.g., a Raman or MRI contrast agent) and as an intrinsic therapeutic agent (e.g., a material that absorbs electromagnetic radiation, converts it to heat, and ablates the cell containing it).

Single-walled carbon nanotubes (SWNTs) are one class of multifunctional nanoparticles that have shown great promise for the imaging and treatment of diseases.³⁻⁶ A SWNT can be represented as a graphene sheet of sp^2 -hybridized carbon atoms seamlessly wrapped into a cylindrical tube. SWNT diameters are typically 0.7 to 1.5 nm, lengths range from 10 nm to several centimeters, and the electronic structure can be metallic or semi-conducting depending on how the graphene sheet is rolled up.⁷⁻¹⁰ Carboxylated SWNTs (C-SWNTs) are particularly well suited for biomedical applications since functional groups on the nanotube surface facilitate the covalent attachment of targeting agents to ensure that the agents remain associated with the SWNT in complex biological environments. Indeed, there are numerous *in vitro* and *in vivo* studies that report the therapeutic effectiveness of covalently-functionalized SWNT constructs with minimal acute toxicity.^{4,6,11-17} Furthermore, in contrast to metal nanoparticles, C-SWNTs have been shown to be biodegraded by neutrophils *in vivo*.¹⁵

Numerous assays are required to accurately evaluate the effectiveness of a targeted

1
2
3 therapy, which depends on many factors including the optimal dose, stability, specificity,
4 toxicity, and degree of cellular internalization.² Many of these assays utilize
5 immunofluorescence detection after the targeting agent is labeled with a fluorescent dye.
6
7 However, in many cases, dye photobleaching limits the use of these assays to short-duration
8 experiments. In contrast, SWNTs make excellent spectroscopic labels because they exhibit
9 persistent Raman scattering, and they are resistant to photobleaching. For example, Cao et al.
10 recently demonstrated an immunoassay detection scheme that used SWNTs as a Raman
11 label.¹⁸ In brief, they adsorbed biotin to the SWNTs and used an avidin-biotin coupling
12 scheme to link the SWNTs to an antibody. Then, SWNT resonances observed in Raman
13 spectra collected from cell extracts of cytomegalovirus-infected fibroblasts were used to
14 detect a primary antibody and a protein antigen with excellent specificity and sensitivity.
15
16 However, imaging whole cells and knowing the cellular distribution of an antibody targeting
17 agent is required to better understand the mechanisms of cellular binding and/or
18 internalization. This is especially important when the antibody is targeted to a membrane
19 receptor overexpressed on a tumor cell. For example, a number of breast cancer therapies
20 involve targeting the human epidermal growth factor receptor 2 (Her2), a transmembrane
21 tyrosine kinase active glycoprotein linked to breast tumor aggressiveness and
22 pathogenesis,^{19,20} using anti-Her2/erB-2 monoclonal antibodies.²¹⁻²³

23
24
25
26
27
28
29
30
31
32
33
34
35
36
37
38
39
40
41
42
43 Today, advances in laser scanning confocal Raman microscopy make it possible to
44 rapidly scan large areas and collect a complete Raman spectrum at every pixel in the image
45 such that cells can be analyzed in a matter of minutes. This technique has been used by our
46 group¹³ and others²⁴ to image the cellular binding and degree of internalization of antibody-
47 SWNT conjugates *in vitro*; furthermore, instruments modified for deep tissue imaging have
48 been used to monitor the accumulation of antibody-SWNT conjugates in tumors *in vivo*.²⁵
49
50
51
52
53
54
55
56 The capabilities of these instruments make them ideally suited to evaluate the efficacy of a
57
58
59
60

1
2
3 SWNT-based therapeutic. For example, we recently used confocal Raman imaging to reveal
4
5 that antibody-SWNT conjugates internalized by tumor cells were more effective therapeutic
6
7 agents than those bound to the surface of tumor cells.¹³
8

9
10 Herein, we expand upon the work of Cao et al.¹⁸ and present a versatile whole-cell
11
12 Raman imaging immunoassay that can evaluate the binding and/or internalization of a tumor
13
14 targeting agent using SWNTs as a Raman label. As a demonstration of the method, we
15
16 evaluated the cellular distribution of Her2 receptors on BT-474 breast tumor cells using Her-
17
18 66, a monoclonal antibody that binds Her2 receptors. Once bound to Her2 receptors, a
19
20 biotinylated secondary antibody is then introduced to bind the primary antibody and to
21
22 provide biotin groups that can link biotinylated C-SWNTs to the secondary antibody via a
23
24 NeutrAvidinTM-FITC bridge (Schemes 1 and 2). This approach enables the binding of the
25
26 targeted C-SWNTs to Her2 receptors to be validated by imaging the distribution of Her2
27
28 receptors on BT-474 cells via immunofluorescence microscopy of NeutrAvidinTM-FITC and
29
30 directly detecting the SWNTs associated with the cells via laser scanning confocal Raman
31
32 microscopy.
33
34
35
36
37
38
39
40
41
42
43
44
45
46
47
48
49
50
51
52
53
54
55
56
57
58
59
60

Materials and methods

(i) Synthesis of biotinylated SWNTs

In brief, SWNTs were oxidized by nitric acid reflux to form C-SWNTs, which were covalently coupled to a tether of (+)-biotinyl-3,6,9-trioxaundecanediamine (biotin-LC-PEO-amine) to form biotinylated-SWNTs (B-SWNTs). Specifically, raw HiPco SWNTs (Lot #R0519, Carbon Nanotechnologies, Inc.) were dispersed in Triton X-100 (TX-100) and refluxed in nitric acid (6 M) for 12 h generating carboxyl groups at the end caps and sidewalls according to a modified procedure involving sonication and centrifugation.²⁶⁻²⁸ The resulting C-SWNTs (0.2 mg) were probe sonicated (VWR Branson Sonifier 250 with a 1/8"-diameter probe tip) continuously for 10 min at 10 W in 1 mL of a 0.1 M 2-(N-morpholino)ethanesulfonic acid buffer, pH 5.0 (MES, 99.5%, Sigma-Aldrich) in a 1.5-mL Eppendorf tube placed in an ice water bath. To remove C-SWNT bundles and other impurities from the samples, the homogeneous black dispersions were centrifuged at a low speed of 700 *g* for 10 min (Eppendorf Centrifuge 5424), the supernatant (950 μ L) was recovered, and the pellet was discarded. The supernatant was centrifuged a second time at 16,000 *g* for 20 min, and 850 μ L of supernatant was collected (the pellet was discarded).

Stock solutions of 1.0 mM biotin-LC-PEO-amine (98%, Pierce Biotechnologies) and 50 mM 1-ethyl-3-(3-dimethylaminopropyl) carbodiimide hydrochloride (EDC, 98%, Pierce Biotechnologies) were prepared by dissolving biotin LC-PEO-amine (0.42 mg) and EDC (9.57 mg) in 1.0 mL of MES buffer. A 2.5 μ L aliquot of the biotin LC-PEO-amine solution (2.5 nmol) and a 100 μ L aliquot of the EDC solution (5 μ mol) were added to the 1.5-mL Eppendorf tube containing C-SWNTs. The mixture was vortexed for 15 s followed by mixing on a rugged rotor Glas-Col (model 099A RD4512) for 2 h at room temperature. The product was centrifuged at 13,000 *g* for 20 min at 4 °C (Beckman TL-100 Ultracentrifuge) to remove unreacted EDC and biotin LC-PEO-amine from the resultant B-SWNTs. The

1
2
3 supernatant was recovered and dialyzed using a 10 kDa molecular weight cut-off dialysis
4 cartridge (Slide-A-Lyzer, Pierce Biotechnologies) for 3 d against 4 L of deionized (DI) water.
5
6
7 The water was changed twice the first day and once each of the remaining days. After
8
9
10 dialysis, the B-SWNT dispersions were characterized by atomic force microscopy (AFM),
11
12 transmission electron microscopy (TEM), UV-Vis-NIR spectrophotometry, and Raman
13
14 spectroscopy. For cell and receptor-mediated immunoassay binding studies, several B-
15
16 SWNT dispersions were pooled and concentrated by solvent evaporation. B-SWNT loadings
17
18 were characterized using sodium dodecyl sulfate-polyacrylamide gel electrophoresis (SDS-
19
20 PAGE).
21
22
23
24

25 **(ii) AFM of SWNT dispersions**

26
27 AFM images were acquired in air under ambient conditions using a Nanoscope III
28
29 Multimode Scanning Probe Microscope operated in the TappingMode™ (Veeco Instruments,
30
31 Inc.). The AFM piezoelectric “J” scanner was calibrated using a Nano Devices Inc. standard,
32
33 and the height calibration was verified using hydrofluoric acid etched pits in muscovite
34
35 mica.²⁹ AFM images for height analysis were acquired using a reduced Z-limit (100-200 V)
36
37 and silicon cantilevers/tips (force constant 5.0 Nm⁻¹, resonant frequency 180 kHz, Veeco
38
39 Instruments, Inc.).³⁰ Aliquots (20 μL) of B-SWNTs and C-SWNTs were spun-cast separately
40
41 onto freshly-cleaved muscovite mica (Asheville-Schoonmaker Mica Co.) at 3,500 rpm for 30
42
43 s. The samples were dried in a desiccator overnight at room temperature prior to imaging.
44
45
46
47
48

49 **(iii) TEM of B-SWNTs labeled with streptavidin gold**

50
51 TEM images of B-SWNTs tagged with streptavidin-coated gold markers (5 nm diameter,
52
53 Kirkegaard and Perry Laboratories Inc.) were obtained using a high contrast Tecnai™ FEI
54
55 G2 Spirit BioTwin transmission electron microscope operated at 120 kV using a LaB₆
56
57
58
59
60

1
2
3 emitter. The instrument is equipped with a 2k × 2k Gatan Ultrascan 1000 multiport CCD
4 camera. Nickel grids (200 mesh, Ted Pella) coated with carbon were used as the support for
5 the samples. The B-SWNT dispersion (100 μL) was treated with 5 μL of a 1:50 dilution of
6 the streptavidin-gold conjugate in DI water and allowed to react for 12 h at room temperature.
7 Following the reaction, the dispersion was ultracentrifuged (Beckman TL-100
8 Ultracentrifuge) twice at 47,000 g for 15 min, and the supernatant containing excess
9 streptavidin-gold conjugate was discarded. The pellet containing streptavidin-gold-labeled
10 B-SWNTs was re-suspended by pipette mixing. The sample (5 μL) was dropped onto a grid,
11 left for 2 min, and the excess was wicked away prior to imaging.
12
13
14
15
16
17
18
19
20
21
22
23
24

25 **(iv) UV-Vis-NIR spectrophotometry of SWNT dispersions**

26 Background-subtracted absorption spectra of TX-100/SWNTs (control sample in D₂O), C-
27 SWNTs (control sample in D₂O), and B-SWNTs (in DI water) were acquired from 400 to
28 1400 nm in 1-mm cuvettes (Suprasil 300, Fisher Scientific) using a dual-beam Perkin-Elmer
29 Lambda 900 UV-Vis-NIR spectrophotometer. The spectra were acquired at a scan speed of
30 125 nm min⁻¹ with a 0.5 s integration time.
31
32
33
34
35
36
37
38
39
40

41 **(v) Raman spectroscopy of SWNT dispersions**

42 Background-subtracted Raman spectra were acquired from C-SWNT and B-SWNT
43 dispersions dried onto glass microscope slides using a WITec alpha 300 series confocal
44 scanning microscope with a 532 nm laser (18 mW) as the excitation source. Wavenumber
45 calibration was performed using the 520.5 cm⁻¹ line of a silicon wafer. The spectral
46 resolution was ~1 cm⁻¹. An area of interest viewed with a 20× objective lens was selected
47 with the software, and spectra (average of 3 spectra) were recorded from 100 to 2000 cm⁻¹.
48
49
50
51
52
53
54
55
56
57
58
59
60

1
2
3 **(vi) SDS-PAGE determination of SWNT concentrations in SWNT dispersions**
4

5 The amounts of C-SWNTs and B-SWNTs used for the binding studies were determined by
6 SDS-PAGE analysis using C-SWNT suspensions as a standard.³¹ The C-SWNT standard
7 was prepared by sonicating C-SWNTs (0.2 mg) in 1.0 mL DI water for 10 min at 10 W
8 constant power. The suspensions were not processed further (*i.e.*, centrifuged) before they
9 were used to generate a standard calibration curve. C-SWNT standards and dispersions and
10 B-SWNT dispersions were loaded in increasing volumes into the gel wells. After
11 electrophoresis at 100 V for 2 h, the pixel intensities of the SWNT-containing dark bands at
12 the loading well/stacking gel interface were scanned using a 16-bit flat bed scanner (9520
13 Photo Scanner, Visioneer) and quantitated using Image Quant software (Image Quant version
14 5.2, GE Healthcare). The concentrations of SWNTs in C-SWNT and B-SWNT dispersions
15 were determined from a linear fit of the C-SWNT standard calibration curve.
16
17
18
19
20
21
22
23
24
25
26
27
28
29
30
31

32 **(vii) Breast ductal carcinoma BT-474 cell culture**
33

34 Breast ductal carcinoma BT-474 cells (American Type Culture Collection, (ATCC),
35 Manassas, VA) were cultured in Hybri-Care culture medium (ATCC) containing 10% fetal
36 calf serum (FCS; HyClone, Logan, UT) and 3.41 g sodium bicarbonate per liter of medium in
37 a 10% CO₂ incubator at 37 °C. The medium was first adjusted to pH 7.2 and then filtered
38 through a 0.2 µm membrane. To determine the number of cells for plating, cells grown in
39 tissue culture dishes were removed with 0.05% trypsin (w/v), and the cell count was
40 determined using a Beckman Coulter Particle Counter (Miami, FL).
41
42
43
44
45
46
47
48
49
50
51

52 **(viii) Immunofluorescence microscopy with BT-474 cells**
53

54 To determine the distribution of the Her2 receptors at 15 °C, the multistep immunoassay
55 (Scheme 1: steps 1 through 4) was performed on live BT-474 cells. Coverslips (12 mm) were
56
57
58
59
60

1
2
3 pretreated with polylysine to allow for better adhesion of the cells to the glass surface and
4
5 placed in 4-well tissue culture (TC) dishes. The BT-474 cells were plated at 8×10^4 cells per
6
7 well on the coverslips, and the cells were grown at 37 °C. Subsequent steps were performed
8
9 entirely at 15 °C, which slows down the rate of endocytic internalization and keeps epitopes
10
11 available to the medium while maintaining good adherence of the cells to the substrate. The
12
13 cells were washed 3 times with phosphate buffered saline (PBS) followed by 10 min
14
15 incubation in PBS containing 10% FCS to block cell surface non-specific binding sites. The
16
17 primary antibody, Her-66, containing 1.47 mg mL^{-1} IgG, was diluted 1:1000 in 10% FCS,
18
19 and a volume of 200 μL was placed on each coverslip. The relative binding affinity of the
20
21 Her-66 antibody on BT474 cells has been reported to be $3.8 \pm 3.2 \times 10^{-9} \text{ M}$.²³ This is the
22
23 concentration necessary to reach 50% saturation of the Her2 receptors. The antibody was
24
25 allowed to bind for 40 min at the appropriate temperature, followed by washing 3 times with
26
27 PBS and blocking with 10% FCS for 10 min. As a nonspecific binding control, the primary
28
29 antibody step was omitted (Scheme 1: steps 1, 3, and 4). The secondary antibody, biotin-
30
31 conjugated goat anti mouse IgG (Pierce, adjusted to a conc. of $1 \mu\text{g mL}^{-1}$), was diluted 1:1000
32
33 in 10% FCS, and 200 μL was placed on each coverslip and allowed to bind for 40 min. The
34
35 excess antibody was removed by washing 3 times with PBS and blocked with 10% FCS for
36
37 10 min. NeutrAvidinTM-FITC (Pierce, 31006 adjusted to a concentration of 5.5 mg mL^{-1})
38
39 was diluted 1:1250 in 10% FCS. A volume of 200 μL was placed on each coverslip and
40
41 allowed to bind for 40 min. The unbound NeutrAvidinTM-FITC was removed by washing the
42
43 cells 3 times with PBS. The cells were fixed with cold 4% paraformaldehyde for 20 min,
44
45 washed 3 times with PBS, and then 3 times with H₂O. The coverslips were mounted on glass
46
47 microscope slides with Fluoromount-GTM preserved with 0.1% NaN₃ (Southern Biotech) and
48
49 viewed with a Nikon Eclipse TE-2000U microscope equipped with a Cascade 512B camera
50
51
52
53
54
55
56
57
58
59
60

1
2
3 and a 60× objective lens (NA = 1.4) (Princeton Instruments). Pixel intensities were adjusted
4
5 to full-scale, and figures were assembled in Adobe Photoshop 5.5 (Adobe Systems).
6
7

8
9
10 **(ix) Confocal Raman imaging of the binding of biotinylated SWNTs to BT-474 cells via**
11 **the immunoassay**
12

13
14 BT-474 cells treated as described above for the immunofluorescence experiments (Scheme 1:
15
16 Steps 1 through 4) at 15 °C were washed and blocked for 10 min with 10% FBS. The
17
18 primary antibody, Her-66 (mouse anti Her2 receptors), secondary antibody (biotinylated goat
19
20 anti-mouse IgG), and NeutrAvidinTM-FITC were introduced at the same concentrations as
21
22 previously described and allowed to bind for 40 min each followed by washing and re-
23
24 blocking with 10% FCS. B-SWNTs (17.5 µg in 180 µL in 10% FCS) were added to each
25
26 cover slip and allowed to bind for 40 min (see Scheme 1: Step 5). The unbound B-SWNTs
27
28 were removed by washing once with 10% FCS and 3 times with PBS. The cells were fixed
29
30 with 4% cold paraformaldehyde (500 µL in each well) at ice bath temperature for 20 min,
31
32 washed 3 times with PBS, washed with DI water, and dried before analysis by Raman
33
34 spectroscopy.
35
36
37

38
39 The B-SWNTs bound to BT-474 cells via the receptor-mediated immunoassay were
40
41 detected with a WITec alpha 300 series confocal Raman microscope. A minimum of 3
42
43 independent Raman images were acquired from a cluster of BT-474 cells (Scheme 1: Steps 1
44
45 through 5) as well as from control cells (in the absence of primary antibody incubation, i.e.,
46
47 Scheme 1: step 2 omitted). Confocal Raman imaging was typically performed on a 70 × 70
48
49 µm area of cells with a 0.3 s integration time for each spectrum (total of 4900 spectra per
50
51 image). Polynomial background subtraction was carried out on the imaged area. The vertical
52
53 resolution was ~1 µm per pixel and the lateral resolution was 350 nm per pixel. The relative
54
55 abundance of targeted B-SWNTs on BT-474 cells was determined by adding all CCD counts
56
57
58
59
60

1
2
3 from the Raman G-band peak (integrated from 1480-1660 cm⁻¹) from each of the 4900
4 spectra in the image using WITec image analysis software. In addition, a series of images
5 was acquired (integration time of 0.2 s, 6mW laser power) from a single BT-474 cell over a
6 depth of approximately 8 μm (z-step = 0.6 μm) after the cell was treated at 15 °C with
7 primary antibody, biotinylated secondary antibody, NeutrAvidinTM-FITC, and B-SWNTs. A
8 reconstructed three-dimensional (3D) image was generated from the G-band region
9 (integrated from 1480-1660 cm⁻¹) of the combined focal stacks using the image analysis
10 software, ImageJ.
11
12
13
14
15
16
17
18
19

20 21 22 **Results and discussion**

23 24 25 **(i) Characterization of C-SWNTs and B-SWNTs**

26 One goal of this work was to create a strong linkage between targeting ligands and the SWNT
27 Raman label. In a fashion similar to the work of Cao et al.,¹⁸ we used the versatile avidin-
28 biotin interaction. However, instead of a non-covalent association between a biotinylated
29 surfactant and SWNTs, we employed C-SWNTs to covalently attach biotin to the Raman
30 label. Specifically, TX-100-dispersed HiPco SWNTs were carboxylated by reflux^{26,27} for 12
31 h in nitric acid; the percent carboxylation of the C-SWNTs was determined by X-ray
32 photoelectron spectroscopy (XPS) to be ~11% atomic (data not shown).²⁸ Next, C-SWNTs
33 were covalently coupled to biotin LC-PEO-amine (Scheme 2) using EDC as a catalyst cross-
34 linker, and excess reagents were removed by dialysis. The overall reaction leads to the
35 formation of amide bonds between the primary amines on the biotin LC-PEO-amine and the
36 carboxyl groups on the C-SWNTs to produce biotinylated SWNTs, termed B-SWNTs.
37
38
39
40
41
42
43
44
45
46
47
48
49
50

51 AFM images were acquired from B-SWNTs to study the distribution of biotin LC-PEO-
52 amine moieties (Fig. 1a). The AFM image shows nodules that were not observed in AFM
53 images of C-SWNTs (Fig. S1), suggesting the presence of biotinylated sites at the ends and
54 sidewalls of the nanotubes. AFM height measurements from bare and coated regions of 18
55
56
57
58
59
60

1
2
3 B-SWNTs were obtained to determine the biotin LC-PEO-amine coating dimensions. The
4
5 difference between the coated SWNT regions (average height = 3.2 ± 1.5 nm; range 1.5-4.0
6
7 nm) and the bare SWNT regions (average height = 0.9 ± 0.3 nm; range 0.5-1.5 nm) was $2.1 \pm$
8
9 0.6 nm. This thickness closely matches the dimensions of the linker provided by Pierce
10
11 (biotin LC-PEO-amine dimension = 2.3 nm), and the average height of the bare regions is
12
13 consistent with the known diameter of individual HiPco SWNTs. Gold nanoparticles (5 nm)
14
15 coated with streptavidin were reacted with B-SWNTs to visualize the distribution of
16
17 biotinylated sites along the SWNT structure using TEM (Fig. 1b). The gold labels observed
18
19 in the TEM image had a similar distribution along the length of the SWNT surface as
20
21 observed in the AFM image. In summary, the combined AFM and TEM results suggest the
22
23 presence of biotin groups at SWNT ends and along sidewalls.
24
25

26
27 UV-Vis-NIR absorption spectrophotometry was used to study the optical transitions of
28
29 the SWNTs in the NIR region before and after biotinylation. Fig. S2 presents UV-Vis-NIR
30
31 absorption spectra of TX-100-dispersed raw HiPco SWNTs, C-SWNTs (12 h of nitric acid
32
33 reflux), and B-SWNTs. The spectrum of TX-100-dispersed SWNTs (Fig. S2a) shows well-
34
35 resolved van Hove singularities indicative of debundled, individually dispersed SWNTs,³²
36
37 whereas the UV-Vis-NIR spectra of C-SWNTs (Fig. S2b) and B-SWNTs (Fig. S2c) show the
38
39 expected loss of optical features indicative of oxidative modification.³³⁻³⁸
40
41

42
43 SDS-PAGE with optical detection was performed according to the procedure developed
44
45 by Wang et al.³¹ to determine the concentrations of SWNTs in C-SWNT and B-SWNT
46
47 dispersions. Three C-SWNT dispersions were prepared with known amounts of C-SWNTs
48
49 (0.2 mg C-SWNT powder per mL) that were not subjected to centrifugation following
50
51 sonication. These C-SWNT dispersions were used to prepare a series of standards for SDS-
52
53 PAGE. The pixel intensities of the bands from these standards were used to generate a
54
55 calibration curve from which the concentrations of SWNTs in the purified C-SWNT and B-
56
57
58
59
60

1
2
3 SWNT dispersions were determined to be $59.5 \pm 4.4 \text{ ng } \mu\text{L}^{-1}$ and $116.7 \pm 4.6 \text{ ng } \mu\text{L}^{-1}$,
4
5 respectively.
6

7 Raman spectroscopy was also performed on C-SWNTs and B-SWNTs. Fig. 2 shows
8 that the Raman spectra of C-SWNTs and B-SWNTs both exhibit characteristic SWNT
9 resonances such as the radial breathing modes (RBMs) ($100\text{-}350 \text{ cm}^{-1}$), the disorder D-band
10 (1350 cm^{-1}), and the tangential G-band (1585 cm^{-1}). In addition, the G-/G+ line shape of the
11 G-band, characteristic of metallic tubes, was observed in the Raman spectra of both C-
12 SWNTs (Fig. 2a) and B-SWNTs (Fig. 2b).
13
14
15
16
17
18
19
20
21
22

23 **(ii) Binding of B-SWNTs on BT-474 cells by immunofluorescence and confocal Raman** 24 **imaging**

25
26 Immunofluorescence microscopy was conducted to determine the location of Her2 receptors
27 on the surface of BT-474 cells. In these experiments, steps 1-4 of Scheme-1 were performed
28 on the surface of BT-474 cells. In these experiments, steps 1-4 of Scheme-1 were performed
29 by incubating cells at $15 \text{ }^\circ\text{C}$ to slow endocytic internalization of receptors. Fig. 3a
30 demonstrates the binding of NeutrAvidinTM-FITC to Her2 receptors on BT-474 cells via the
31 linkage provided by the biotinylated secondary antibody and the primary antibody. A
32 representative immunofluorescence imaging stack acquired from a single BT-474 cell over a
33 depth of $8 \text{ } \mu\text{m}$ after performing the immunoassay is shown in Fig. S3a. As the focal plane
34 progressed through the cell, there was modest fluorescence once past the cell surface,
35 consistent with the idea that endocytosis is slow at $15 \text{ }^\circ\text{C}$ and that the receptors could still be
36 seen on the cell surface. As a control, incubation was carried out while omitting the primary
37 antibody from the immunoassay scheme (skipping step 2 in Scheme 1). In the absence of the
38 primary antibody, only background fluorescence is observed due to insignificant nonspecific
39 binding of NeutrAvidinTM-FITC to BT-474 cells (Fig. 3b).
40
41
42
43
44
45
46
47
48
49
50
51
52
53
54
55
56
57
58
59
60

1
2
3 Confocal Raman studies were performed on BT-474 cells following the binding
4 immunoassay with B-SWNTs (Scheme 1: steps 1-5). Figs. 3c and 3d show optical and 3D
5 Raman images, respectively, of the same BT-474 cell following treatment with the primary
6 antibody, the biotinylated secondary antibody, NeutrAvidinTM-FITC, and the B-SWNTs at
7 15 °C. The bright yellow areas in (d) correspond to G-band intensities (integrated from
8 1480-1660 cm⁻¹) acquired from each 1-μm² pixel in the image. Since cells not exposed to
9 SWNTs did not show any detectable Raman signals in the G-band region (data not shown),
10 the G-band can be used as a direct measure of the presence of SWNTs. The similarity in the
11 distribution of labels observed in the immunofluorescence (Fig. 3a) and 3D Raman images
12 (Fig. 3d) indicates that the binding of NeutrAvidinTM-FITC to Her2 receptors via the linkage
13 between the biotinylated secondary antibody and the primary antibody (Fig. 3a) correlates
14 with the binding of B-SWNTs to Her2 receptors via the linkage of the NeutrAvidinTM-FITC,
15 biotinylated secondary antibody, and primary antibody (Fig. 3d). A major advantage of
16 confocal Raman imaging is the ability to view different focal planes within a cell. After
17 performing the binding immunoassay, a Raman spectrum was acquired from a cellular region
18 (Fig. S3c), and a stack of 12 focal images from the cell (Fig. S3b), each separated by 0.6 μm
19 in the z-direction, was assembled in 3D (Fig. 3d) to show the targeting of B-SWNTs for Her2
20 receptors. The sequential Raman images suggest that B-SWNTs are located on the surface
21 and inside the cells, consistent with slow endocytosis at 15 °C. These results are similar to
22 the immunofluorescence results in Fig. S3a.

23
24
25
26
27
28
29
30
31
32
33
34
35
36
37
38
39
40
41
42
43
44
45
46
47 To further demonstrate specificity, additional confocal Raman studies were performed on
48 BT-474 cells at 15 °C following the binding immunoassay with B-SWNTs (Scheme 1: steps
49 1-5) either with (Figs. 4a and 4b) or without (Figs. 4c and 4d) the primary antibody. Fig. 4b
50 again shows an intense Raman G-band signal from the surface binding of B-SWNTs to Her2
51 receptors on BT-474 cells at 15 °C via the linkage provided by NeutrAvidinTM-FITC, the
52
53
54
55
56
57
58
59
60

1
2
3 biotinylated secondary antibody, and the primary antibody. When the primary antibody was
4
5 omitted, there was a reduced Raman signal (Fig. 4d) suggesting a minor amount of non-
6
7 specific binding. Fig. 4e shows a Raman spectrum obtained from a high intensity area in the
8
9 confocal Raman image (Fig. 4b) in which the strong G-band signal directly confirms the
10
11 presence of SWNTs. Fig. 4f shows a Raman spectrum obtained from the control cells (Fig.
12
13 4d), which reflects a small amount of non-specific signal in the Raman image, in particular,
14
15 the small peak at $\sim 1570\text{-}1610\text{ cm}^{-1}$.
16
17

18
19 To estimate the amount of B-SWNTs bound to Her2 receptors on the BT-474 cells at 15
20
21 $^{\circ}\text{C}$, the Raman G-band intensities measured from spectra associated with the image pixels
22
23 were summed. The average Raman intensity for the specific binding of B-SWNTs to BT-474
24
25 cells at 15 $^{\circ}\text{C}$ was $1.10 \pm 0.07 \times 10^8$ CCD counts per cell as compared to $0.07 \pm 0.04 \times 10^8$
26
27 CCD counts per cell for the control sample without primary antibody. This 94% reduction in
28
29 Raman signal indicates that there was minimal non-specific binding of B-SWNTs to BT-474
30
31 cells at 15 $^{\circ}\text{C}$ in the absence of the primary antibody.
32
33

34
35 Further evidence that the distribution of B-SWNTs represents targeting of Her-66 to
36
37 Her2 receptors was provided by performing cell uptake studies for 3 d with non-targeted
38
39 SWNTs at 37 $^{\circ}\text{C}$, conditions under which the SWNTs are internalized by fluid-phase
40
41 endocytosis and are delivered to lysosomes.³⁸ BT-474 cells were incubated with C-SWNTs
42
43 (0.2 mg mL^{-1}) in media for 3 d at 37 $^{\circ}\text{C}$ followed by confocal Raman microscopy to image
44
45 the C-SWNTs. Figure 5 shows an optical image (Fig. 5a) and the corresponding confocal
46
47 Raman image (Fig. 5b) of the same BT-474 cell cluster that had internalized C-SWNTs. The
48
49 perinuclear distribution of non-targeted SWNTs (Fig. 5b) suggests that the majority of the
50
51 non-targeted SWNTs are within intracellular vesicles, probably lysosomes, consistent with
52
53 the long uptake time at 37 $^{\circ}\text{C}$ used in this experiment.
54
55
56
57
58
59
60

Conclusion

In this article, we demonstrated a carbon nanotube-based Raman-imaging immunoassay for evaluating tumor-targeting ligands. The assay used biotinylated-SWNTs as a Raman label, avidin-biotin chemistry to link the Raman label to a receptor-targeting ligand, and confocal Raman microscopy to image whole cells. Using a breast tumor cell model, we demonstrated the usefulness of the method to assess membrane receptor/ligand systems by evaluating a monoclonal antibody, Her-66, known to target overexpressed Her2 receptors. The overall approach is versatile such that one could easily study and screen other targeting antibodies such as the Her-50 and Her-81 antibodies used by Marches et al.,¹³ and rank them in order of efficacy of targeting. Additionally, we analyzed Raman images acquired from different focal planes within a single BT-474 cell. We found that the cellular distribution of the SWNT label, which corresponds to the distribution of Her2 receptors, suggests that the targeted SWNT complexes were present on the surface of BT-474 cells. The ability to image the interaction of targeting ligands should find widespread use in elucidating mechanisms of ligand-receptor interactions towards the pre-clinical optimization of a variety of targeted nanotube constructs.

Acknowledgements

This work was supported by SEMATECH/Semiconductor Research Corporation (grant ERC425-042), the Human Frontier Science Program (grant #RCY0070/2005-C), DOD (grant W81XWH-08-20004), the Texas Higher Education Coordinating Board Advanced Technology Program, and the Center for Applied Biology at The University of Texas at Dallas. We also thank Ellen S. Vitetta, Radu Marches, and Pavitra Chakravarty (UT Southwestern Center for Cancer Immunobiology) for helpful discussions and the Her-66

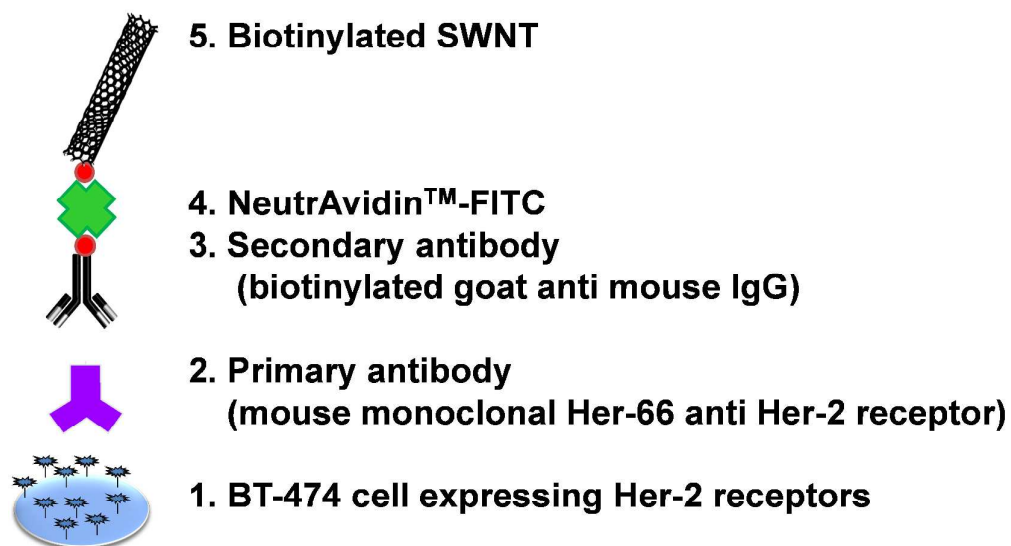
1
2
3 monoclonal antibody, and Chris Gilpin (UT Southwestern Molecular and Cellular Imaging
4
5 Facility) for assistance with electron microscopy.
6
7
8
9
10
11
12
13
14
15
16
17
18
19
20
21
22
23
24
25
26
27
28
29
30
31
32
33
34
35
36
37
38
39
40
41
42
43
44
45
46
47
48
49
50
51
52
53
54
55
56
57
58
59
60

References

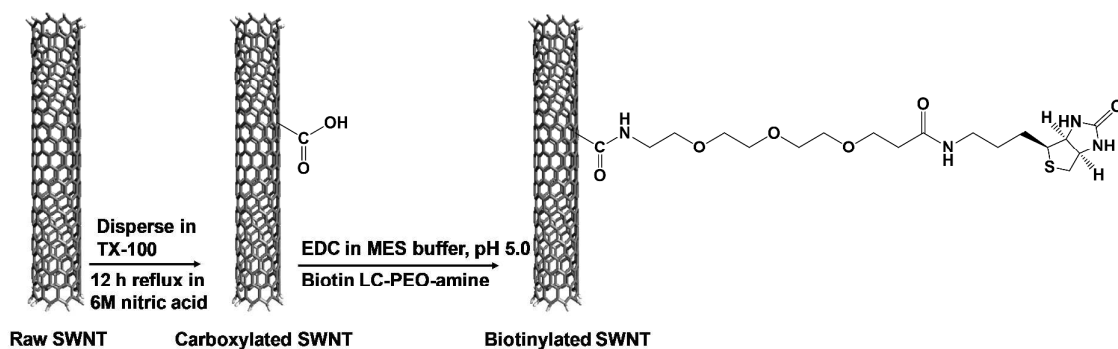
1. D. E. Gerber, *Amer. Fam. Phys.* 2008, **77**, 311-319.
2. Y. Yan, G. K. Such, A. P. R. Johnston, J. P. Best, and F. Caruso, *ACS Nano*, 2012, **6**, 3663-3669.
3. M. Foldvari, and M. Bagonluri, *Nanomedicine: Nanotechnol. Biol. Medicine*, 2008, **4**, 173-200.
4. Z. Liu, S. Tabakman, K. Welsher, and H. Dai, *Nano Res.*, 2009, **2**, 85-120.
5. S. R. Ji, C. Liu, B. Zhang, F. Yang, J. Xu, J. Long, C. Jin, D.L. Fu, Q.X. Ni, and X. J. Yu, *Biochim. Biophys. Acta Reviews on Cancer*, 2010, **1806**, 29-35.
6. C. Fabbro, H. Ali-Boucetta, T. Da Ros, K. Kostarelos, A. Bianco, and M. Prato, *Chem. Commun.*, 2012, **48**, 3911-3926.
7. M. S. Dresselhaus, G. Dresselhaus, A. Jorio, A. G. Souza Filho, and R. Saito, *Carbon*, 2002, **40**, 2043-2061.
8. R. H. Baughman, A. A. Zakhidov, and W. A. de Heer, *Science*, 2002, **297**, 787-792.
9. M. Ouyang, J.-L. Huang, and C. M. Lieber, *Acc. Chem. Res.*, 2002, **35**, 1018-1025.
10. P. Avouris, *Acc. Chem. Res.*, 2002, **35**, 1026-1034.
11. Y. Xiao, X. Gao, O. Taratula, S. Treado, A. Urbas, R. D. Holbrook, R. E. Cavicchi, C. T. Avedisian, S. Mitra, R. Savla, P. D. Wagner, S. Srivastava, and H. He, *BMC Cancer*, 2009, **9**, 351-361.
12. R. Marches, P. Chakravarty, I. H. Musselman, P. Bajaj, R. N. Azad, P. Pantano, R. K. Draper, and E. S Vitetta, *Int. J. Cancer*, 2009, **125**, 2970-2977.
13. R. Marches, C. Mikoryak, R. Wang, P. Pantano, R. K. Draper, and E. S. Vitetta, *Nanotechnology*, 2011, **22**, 095101.
14. M. A. Herrero, L. Lacerda, A. Bianco, K. Kostarelos, and M. Prato, *Int. J. Nanotechnology*, 2011, **8**, 885-897.

- 1
2
3 15. V.E. Kagan, N. V. Konduru, W. Feng, B. L. Allen, J. Conroy, Y. Volkov, I. I. Vlasova,
4
5 N. A. Belikova, N. Yanamala, A. Kapralov, Y. Y. Tyurina, J. Shi, E. R. Kisin, A. R.
6
7 Murray, J. Franks, D. Stolz, P. Gou, J. K.Seetharaman, B. Fadeel, A. Star, and A. A.
8
9 Shvedova, *Nature Nanotechnol.*, 2010, **5**, 354-359.
10
11
12 16. B. Sitharaman and L. J. Wilson, *Intl. J. Nanomed.*, 2006, **1**, 291-295.
13
14 17. J. H. Choi, F. T. Nguyen, P. W. Barone, D. A. Heller, A. E. Moll, D. Patel, S. A. Boppart,
15
16 and M. S. Strano *Nano Lett.*, 2007, **7**, 861-867.
17
18 18. C. Cao , J. H. Kim, Y. J. Kwon, Y. J. Kim, E. S. Hwang, and S. Baik, *Analyst*, 2009, **134**,
19
20 1294-1296.
21
22
23 19. Y. Yarden, *Oncology*, 2001, **61**, 1-13.
24
25 20. S. Ménard, E. Tagliabue, M. Campiglio, and S. M. Pupa, *J. Cell. Physiol.*, 2000, **182**,
26
27 150-162.
28
29 21. C. F. Singer, W. J. Köstlerband, and G. Hudelist, *Biochim. Biophys. Acta.*, 2008, **1786**,
30
31 105-113.
32
33 22. L. Z. Lee, Y. Wang, H. Y. Cheng, S. Pervaiz, and Y. Y. Yang, *Biomaterials*, 2009, **30**,
34
35 919-927.
36
37 23. C. I Spiridon, M. A. Ghetie, J. Uhr, R. Marches, J. L. Li, G. L. Shen, and E. S. Vitetta,
38
39 *Clin. Cancer Res.* 2002, **8**, 1720-1730.
40
41
42 24. C. Lamprecht, N. Gierlinger, E. Heister, B. Unterauer, B. Plochberger, M. Brameshuber,
43
44 P. Hinterdorfer, S. Hild, and A. Ebner, *J. Phys. Condens. Matter*, 2011, **24**, 164206.
45
46 25. C. Zavaleta, A. de la Zerda, Z. Liu, S. Keren, Z. Cheng, M. Schipper, X. Chen, H. Dai,
47
48 and S. S. Gambhir, *Nano Lett.*, 2008, **8**, 2800-2805.
49
50
51 26. M. N. Tchoul, W. T. Ford, G.Lolli, D. E. Resasco, and S. Arepalli, *Chem. Mater.*, 2007,
52
53 **19**, 5765-5772.
54
55
56 27. H. Hu, B.Zhao, M. E. Itkis, and R. C. Haddon *J. Phys. Chem. B*, 2003 **107**, 13838-13842.
57
58
59
60

- 1
2
3 28. (a) P. Bajaj, M.S Thesis, The University of Texas at Dallas, 2008. (b)
4
5 P. Bajaj, Ph.D. Dissertation, The University of Texas at Dallas, 2010.
6
7
8 29. L. A. Nagahara, K. Hashimoto, and A. Fujishima, *J. Vac. Sci. Technol. B.*, 1994, **12**,
9
10 1694-1697.
11
12 30. V. Z. Poenitzsch, and I. H. Musselman, *Microsc. Microanal.*, 2006, **2**, 221-227.
13
14 31. R. Wang, C. Mikoryak, E. Chen, S. Li, P. Pantano, and R. K. Draper, *Anal. Chem.*, 2009,
15
16 **15**, 2944-2952.
17
18 32. M. J. O'Connell, S. M. Bachilo, C. B. Huffman, V. C. Moore, M. S. Strano, E. H. Haroz,
19
20 K. L. Rialon, P. J. Boul, W. H. Noon, C. Kittrell, J. Ma, R. H. Hauge, R. B. Weisman,
21
22 and R. E. Smalley, *Science* 2002, **297**, 593-596.
23
24 33. M. E. Itkis, S. Niyogi, M. E. Meng, M. A. Hamon, H. Hu, and R. C. Haddon, *Nano Lett.*,
25
26 2002, **2**, 155-159.
27
28 34. A. Hartschuh, H. N. Pedrosa, J. Peterson, L. Huang, P. Anger, H. Qian, A. J. Meixner, M.
29
30 Steiner, L. Novotny, T. D. Krauss, *Chem. Phys. Chem.* 2005, **6**, 1-6.
31
32 35. J. L. Bahr, and J. M. Tour, *J. Mater. Chem.*, 2002, **12**, 1952-1958.
33
34 36. C. A. Dyke, and J. M. Tour, *Chem. Eur. J.*, 2004, **10**, 812-817.
35
36 37. B. Zhao, M. E. Itkis, S. Niyogi, H. Hu, J. Zhang, and R. C. Haddon, *J. Phys. Chem. B*
37
38 2004, **108**, 8136-8141.
39
40 38. R. Wang, C. Mikoryak, S. Li, D. Bushdiecker II, I. H. Musselman, P. Pantano, and R. K.
41
42 Draper, *Mol. Pharmaceutics* 2011, **8**, 1351-1361.
43
44
45
46
47
48
49
50
51
52
53
54
55
56
57
58
59
60



Scheme 1. Schematic diagram of the immunoassay for the binding of a biotinylated SWNT (B-SWNT) to a breast tumor (BT-474) cell. The specific binding of the mouse monoclonal Her-66 antibody to Her2 receptors on the BT-474 cells is followed by the introduction of a biotinylated secondary antibody that binds to the B-SWNT via a biotin-avidin-biotin bridge.



Scheme 2. Schematic diagram of the SWNT carboxylation and biotinylation reactions. HiPco SWNTs dispersed by TX-100 were refluxed in nitric acid to yield carboxylated SWNTs (C-SWNTs), which were reacted with biotin LC-PEO-amine to yield biotinylated SWNTs (B-SWNTs).

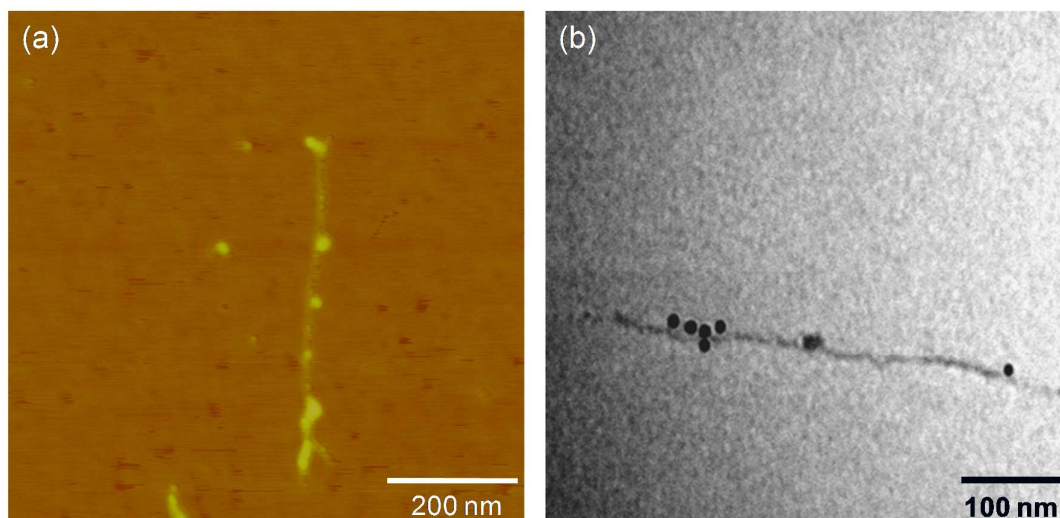


Fig. 1. (a) AFM image (800×800 nm) of B-SWNTs where the bright nodules denote the attachment of biotin LC-PEO-amine to C-SWNTs, and (b) TEM image of a streptavidin gold-labeled SWNT-biotin LC-PEO-amine conjugate, where the solid black spheres mark the attachment of streptavidin-gold to biotin sites on the B-SWNT.

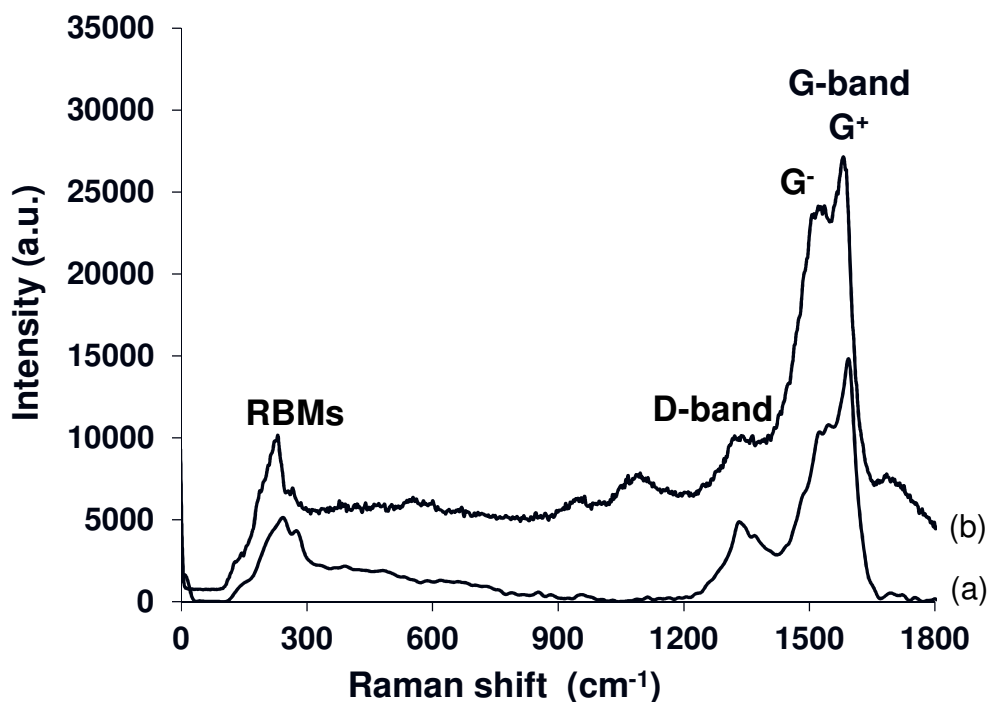


Fig. 2. Raman spectra (laser excitation wavelength 532 nm) of (a) C-SWNTs and (b) B-SWNTs showing characteristic SWNT resonances such as the radial breathing modes (RBMs) between 100-350 cm⁻¹, the disorder D-band at 1350 cm⁻¹, and the tangential G-band at 1585 cm⁻¹.

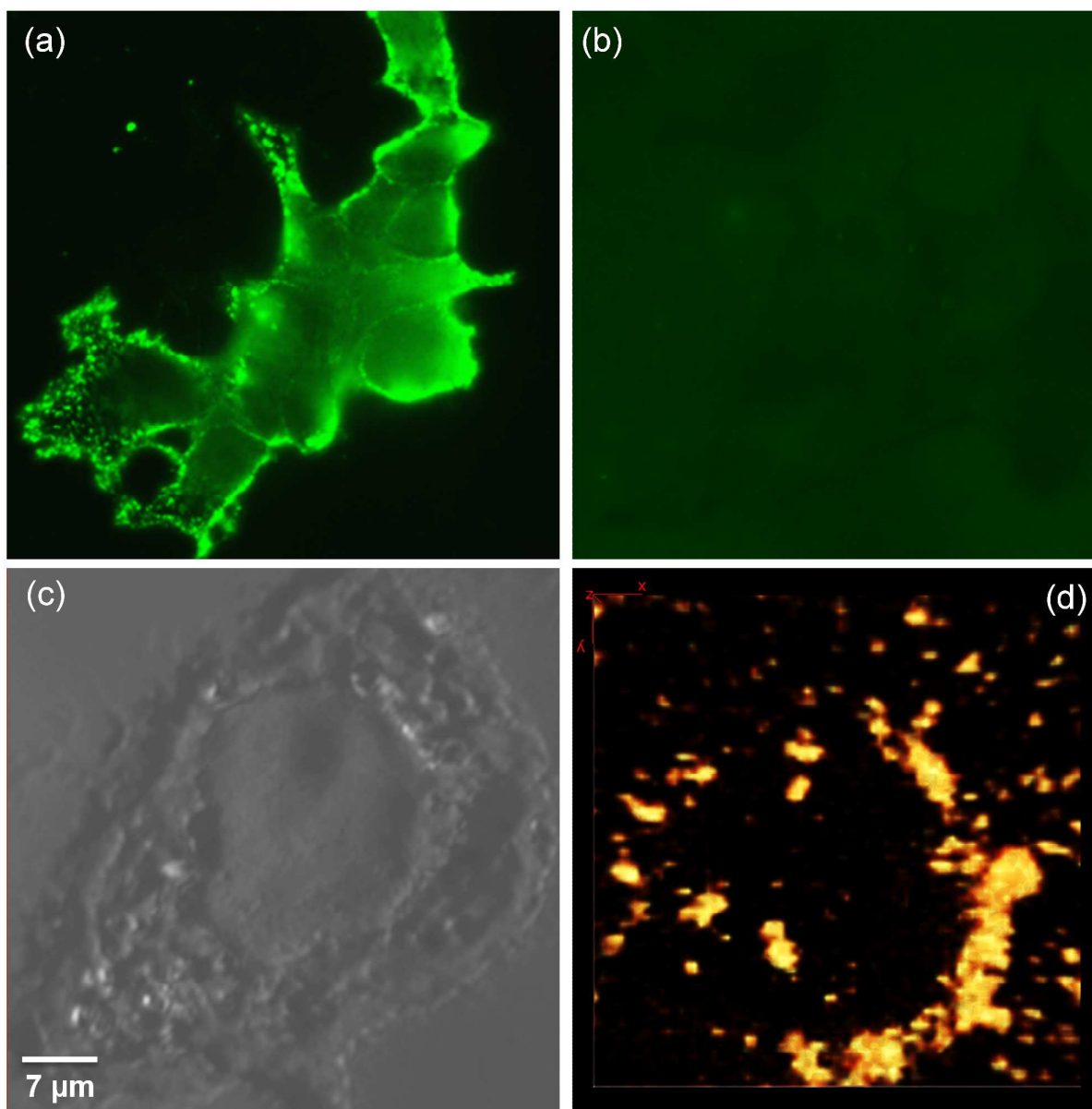


Fig. 3. Immunofluorescence images (normalized to the same color scale) showing (a) the specific binding of NeutrAvidinTM-FITC to Her2 receptors on BT-474 cells following treatment with primary antibody, biotinylated secondary antibody, and NeutrAvidinTM-FITC at 15 °C, and (b) as a control, the binding of NeutrAvidinTM-FITC to Her2 receptors in the absence of the primary antibody at 15 °C. (c) Bright field optical image of the BT-474 cell analyzed. (d) A WITec Alpha 300 scanning confocal microscope was used to acquire 12 two-dimensional Raman images of the same BT-474 cell each at a different focal plane over

1
2
3 an approximate 8 μm cell depth with a z-step of 0.6 μm following treatment with B-SWNTs,
4
5 NeutrAvidinTM-FITC, biotinylated secondary antibody, and the primary antibody at 15 °C. A
6
7 3D reconstructed volume was generated from the G-band region of the 12 combined stacks
8
9 using ImageJ analysis software. The bright yellow areas in (d) correspond to G-band
10
11 intensities (integrated from 1480-1660 cm^{-1}) acquired from each 1- μm^2 pixel in the image
12
13 shown on a color intensity scale where yellow is the highest intensity and black is the lowest.
14
15
16
17
18
19
20
21
22
23
24
25
26
27
28
29
30
31
32
33
34
35
36
37
38
39
40
41
42
43
44
45
46
47
48
49
50
51
52
53
54
55
56
57
58
59
60

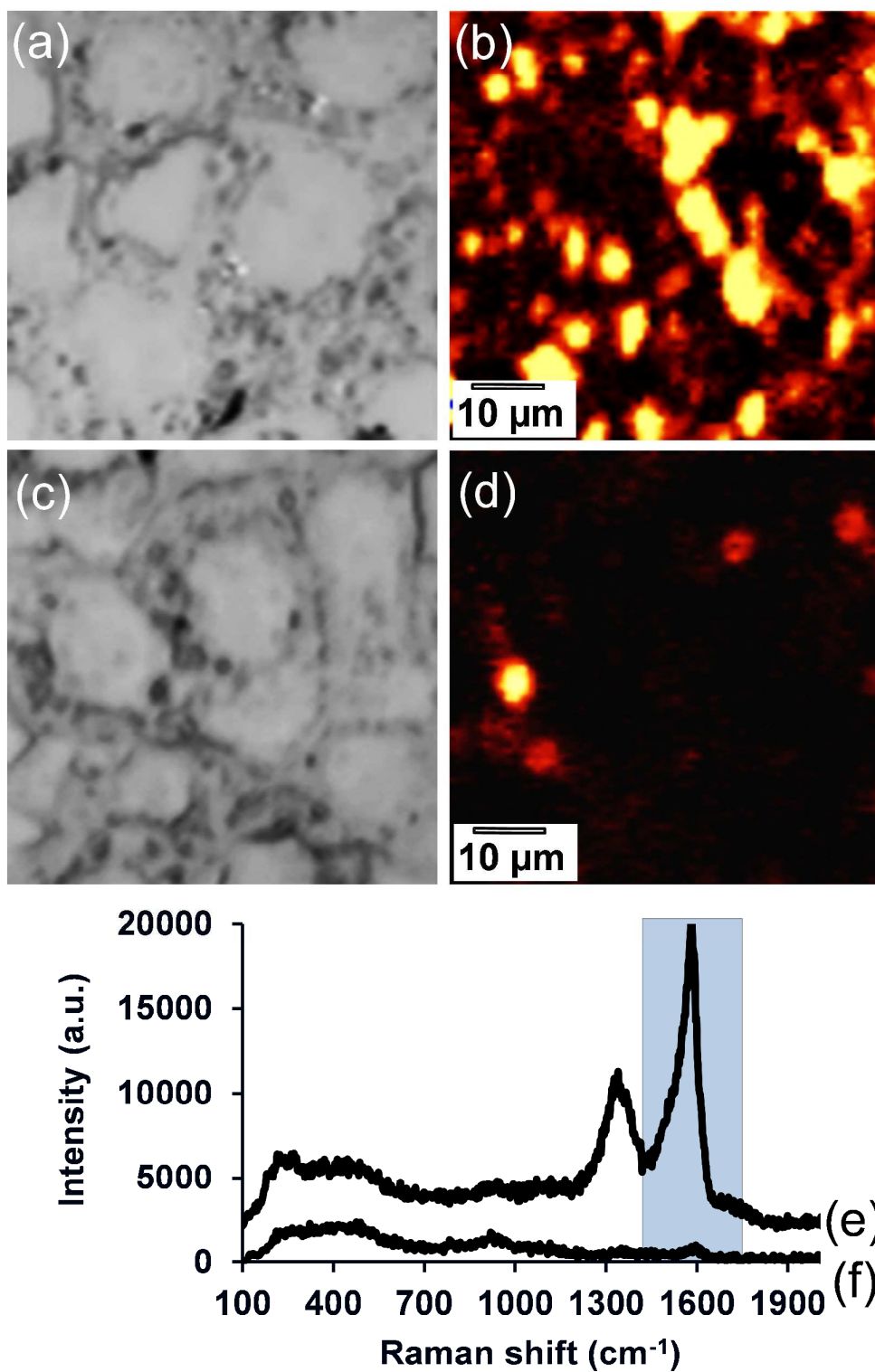


Fig. 4. Optical (a) and Raman (b) images ($70 \times 70 \mu\text{m}$) of the same BT-474 cell cluster following treatment with B-SWNTs, NeutrAvidinTM-FITC, the biotinylated secondary

1
2
3 antibody, and the primary antibody at 15 °C. The yellow areas in (b) correspond to G-band
4
5 intensities (integrated from 1480-1660 cm^{-1}) acquired from each $1\text{-}\mu\text{m}^2$ pixel in the image.
6
7 The representative Raman spectrum (e) acquired from the cellular region in (b) displays the
8
9 characteristic G-band signature of SWNTs. Optical (c) and Raman (d) images ($70 \times 70 \mu\text{m}$)
10
11 of a different BT-474 cell cluster following the same immunoassay steps at 15 °C except that
12
13 the primary antibody was omitted (control). The representative Raman spectrum (f) acquired
14
15 from the cellular region in (d) displays a negligible G-band when the primary antibody is
16
17 omitted. Spectra (e) and (f) were normalized to the same intensity scale, and images (b) and
18
19 (d) were normalized to the same color scale.
20
21
22
23
24
25
26
27
28
29
30
31
32
33
34
35
36
37
38
39
40
41
42
43
44
45
46
47
48
49
50
51
52
53
54
55
56
57
58
59
60

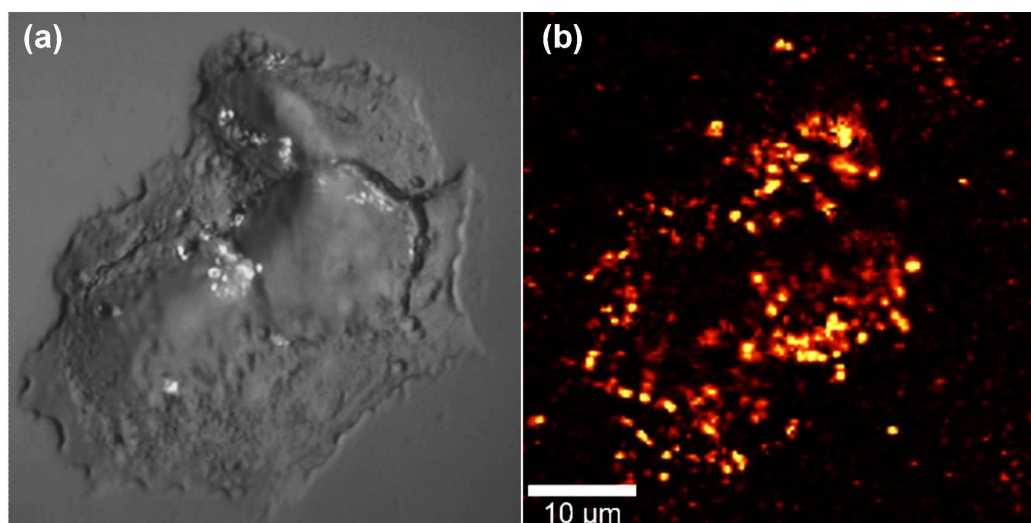


Fig. 5. Optical (a) and Raman (b) images ($50 \times 50 \mu\text{m}$) of the same BT-474 cells following incubation with C-SWNTs for 3 d at 37°C . The bright yellow areas in (b) correspond to G-band intensities (integrated from $1480\text{-}1660 \text{ cm}^{-1}$) acquired from each $1\text{-}\mu\text{m}^2$ pixel in the image.